Immobilisation of uranium-contaminated liquid waste in an alkali-activated material (AAM) and subsequent leaching behaviour

Mooren, Evangelia D.; Bonani, Walter; Popa, Karin; Van Winckel, Stefaan; Alvarez-Sarandes, Rafael; Konings, Rudy J.M.; Beersaerts, Glenn; Schreurs, Sonja; Schroeyers, Wouter

DOI
10.1007/s10967-025-10111-4

Publication date
2025

Document Version
Final published version

Published in
Journal of Radioanalytical and Nuclear Chemistry

Journal of Radioanalytical and Nuclear Chemistry (2025) 334:3505–3516
https://doi.org/10.1007/s10967-025-10111-4

Immobilisation of uranium-contaminated liquid waste in an alkali-activated material (AAM) and subsequent leaching behaviour

Evangelia D. Mooren[1,2] · Walter Bonani[1] · Karin Popa[1] · Stefaan Van Winckel[1] · Rafael Alvarez-Sarandes[1] · Rudy J. M. Konings[1,3] · Glenn Beersaerts[4] · Sonja Schreurs[2] · Wouter Schroeyers[2]

Received: 15 January 2025 / Accepted: 28 March 2025 / Published online: 21 April 2025

Abstract

We present a two-step procedure for treating contaminated liquid waste generated during the processing of uranium, specifically residual uranium-contaminated liquid after precipitation. After precipitating U(IV) as sodium diuranate under alkaline conditions, the resulting solution was solidified by immobilising it in an alkali-activated material. Static leaching tests indicated excellent material stability in water. Exposing the material to aggressive chemical conditions (nitric acid) resulted in slow and incomplete dissolution of uranium (and of structural elements) from a thin superficial layer with further passivation. Characterisation of the solid phase was performed to assess the stability of the alkali-activated material under the tested conditions.

Graphical abstract

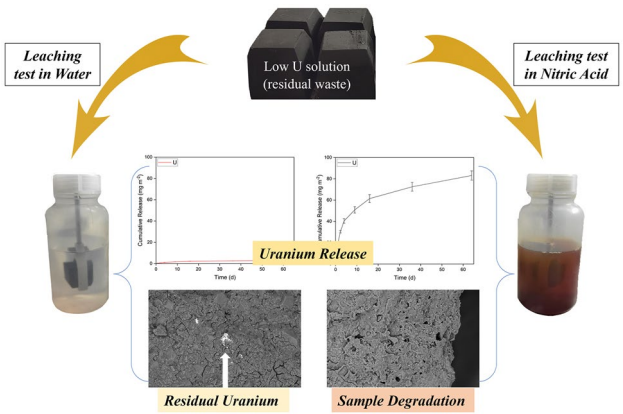

Keywords Alkali activated materials · Monolithic leaching · Liquid radioactive waste · Uranium immobilisation

✉ Walter Bonani
Walter.BONANI@ec.europa.eu

✉ Karin Popa
Karin.POPA@ec.europa.eu

[1] Joint Research Centre, European Commission, Karlsruhe, Germany

[2] Present Address: Faculty of Engineering Technology, Nuclear Technological Centre (NuTeC), CMK, Hasselt University, Agoralaan, Gebouw H, 3590 Diepenbeek, Belgium

[3] Faculty of Applied Sciences, Radiation Science & Technology Department, Delft University of Technology, Mekelweg 15, 2629JB Delft, The Netherlands

[4] Department of Materials Engineering, KU Leuven, Kasteelpark Arenberg 44, 3001 Leuven, Belgium

Introduction

Uranium is a natural component of the environment, with average concentrations of 2.7 ppm in the earth's crust and 3.3 ppb in seawater [1]. However, due to extensive activities related to the front end of the nuclear fuel cycle, remediation of uranium contamination in the environment is a global concern [2–4]. Furthermore, large volumes of radioactive wastewater have been released into the environment as a result of the uranium mining industry's explosive growth and intensive mining and processing operations. This has contaminated surface and groundwater and presented major health and environmental dangers [5, 6]. The chemistry of this element is very complex and strongly depends on a multitude of factors. In an undisturbed geological ore deposit, uranium is mostly present as immobile U(IV) compounds. In the presence of atmospheric oxygen (and water), it is oxidized to far more soluble U(VI) compounds [7]. Other factors influencing the uranium speciation are the temperature, pressure, pH, salinity, presence of radiolytic peroxide or of microbiologic activity [8, 9].

The front end of the nuclear fuel cycle is the main anthropogenic source of uranium in the environment. Historically, tailings from uranium mining and milling were stored and disposed of without properly addressing the associated health and safety issues [10]. These tailings contain the decay products of the ^{238}U and ^{235}U decay chains, including highly active isotopes of radium, radon (gaseous), bismuth, and polonium.

The current regulations establish low limits for the release of uranium and uranium compounds in effluents (*e.g.* [11].). For instance, the guideline values for uranium in drinking water are in the range of 15–30 ppb [12], while for industrial effluents these values can be several orders of magnitude larger [13, 14].

Physical immobilisation of uranium has been established via conventional solidification/stabilisation (S/S) remediation technology, using Ordinary Portland Cement (OPC). However, by releasing cementitious hydrates and calcium hydroxide, exposure to groundwater can weaken the structure of hydrated cement and perhaps result in the creation of soluble UO_2–CO_3 species [15, 16].

Inorganic aluminosilicate compounds known as alkali-activated materials (AAMs) have drawn a lot of interest lately due to their possible use in the immobilisation of radioactive waste [17]. Various studies have shown that geopolymers, a classification of AAMs, have more favourable properties for nuclear waste immobilisation than OPC [18–21]. The ability of geopolymers to successfully retain and immobilise radionuclides such as strontium and caesium is a crucial aspect of their application for radioactive waste treatment [22–24]. An essential component of assessing AAMs' long-term efficacy as a radioactive waste immobilisation matrix is conducting monolithic leaching experiments [25]. Furthermore, AAMs have been shown to be less susceptible [26] as well as less prone to deterioration due to acid attacks [27] compared to OPC.

In this work, we are presenting a two-step approach for treating aqueous waste containing uranium. After treatment and immobilisation in an alkali-activated material, we tested the solid compound by leaching in water and in acidic conditions, to assess its suitability for the intermediate and final disposal of nuclear waste.

Experimental

To overcome the wide variation in concentration, pH, and competing ions in the waste solutions produced in our labs, we are presenting the results obtained based on a model uranium solution with well-defined characteristics. Thus, an aqueous solution of uranyl nitrate ($UO_2(NO_3)_2$) with a concentration of 19.77 g L^{-1} was made from a concentrated stock solution by appropriate dilution, mimicking an institutional uranium waste stream.

Stage 1: Alkaline precipitation and reconversion of uranium

Using a magnetic stirrer, 0.8 g of sodium hydroxide (NaOH) pellets (Bernd Kraft GmbH), was slowly dissolved in 250 mL distilled water containing 1.6 g of the $UO_2(NO_3)_2$ solution mentioned above (11.9 mg U respectively), until the mixture reached a pH of 13.5. The formation of sodium diuranate ($Na_2U_2O_7$) became visible as the transparent solution changed from a pale yellow colour to a cloudy, intense yellow. The suspension was left overnight, and the $Na_2U_2O_7$ precipitate settled to the bottom of the beaker. Then the mixture was filtered with filter paper (Schleicher & Schuell, nr. 595) and the filtrate was recovered. Stage 1, the precipitation of U (Fig. 1), contributes to waste minimisation as most of the U is retained in a low-volume solid phase. It is important to consider that during the filtration U colloids that are still in suspension can pass through the pores of the filter and flocculate with time. The sodium diuranate precipitate can be converted to an oxide form by thermal treatment at a temperature above 1000 °C [28].

Stage 2: Immobilisation in alkali-activated material

The clear supernatant was analysed with a high-resolution inductively coupled plasma optical emission spectroscopy (HR-ICP-OES) instrument (Ultima2, HORIBA JobinYvon) The measured concentration of sodium (Na) was 0.1 mol L^{-1}

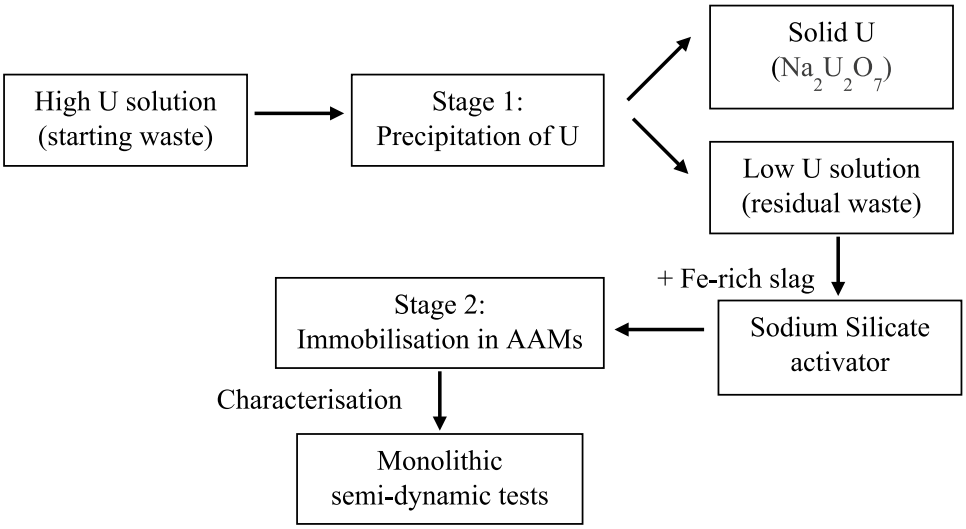

Fig. 1 Uranium removal process in waste treatment

and the concentration of uranium (U) was $1.33 \cdot 10^{-4}$ mol L^{-1} (0.0317 g L^{-1}). Note that the actual concentration of uranium in the AAM samples (of 186.8 µg g^{-1}) was larger than the one expected from the measurement of residual solution due to the contribution of the particulate matter. To obtain the actual concentration of U in the AAM samples 1 g of AAM powderised sample was suspended in 25 mL of HNO_3 65% (14 M concentration) for 24 h with intermediate shaking. The solution was filtered with a 0.2 µm syringe filter (Whatman™ Puradisc™) and measured with ICP-MS for its U content. The results were used to calculate the true concentration of U in the samples.

A synthetic slag was preferred over commercially available slags to simplify the elemental content of the material. Precise amounts of pure SiO_2, Al_2O_3, CaO, and Fe_xO_y powders were mixed into a homogenous mixture to form the synthetic slag rich in Fe, Si, Ca, and Al oxides. After that, the mixture was heated to 1250 °C in an induction furnace (Indutherm TF4000). The combination was first melted in an argon (Ar) environment. Once the melting process started, CO/CO_2 was added. The mixture was kept at room temperature in a reducing atmosphere for 30 min after total melting. After that, the slag was water quenched to cool the molten slag. After the slag was quenched, it was dried for 24 h at 110 °C and then ground into a powder using an attritor (1S Wiener) with a specific surface area of around 3800 g cm^{-2}. Table 1 presents the composition as determined by X-Ray Fluorescence utilising a Bruker axs S8 Tiger spectrometer. Prior to the XRF measurement, the slag was dried at 100 °C for a whole night.

A sodium silicate solution (130 g) was prepared with molar ratios $SiO_2/Na_2O = 1.6$ and $H_2O/Na_2O = 25$. The activator solution was made by combining the U-contaminated supernatant produced after segregating the $Na_2U_2O_7$, pure NaOH pellets (Sodium hydroxide, Pellets, Pure, Bernd Kraft GmbH), and a commercial silicate solution (molar ratio $SiO_2/Na_2O = 3.48$, 65 wt% H_2O, Supelco, Merck).

The AAM samples were prepared by mixing the precursor slag (300 g) with the U-contaminated activator (117 g) with a solution/slag mass ratio of 0.39. After homogenising the mixture, it was transferred to $25 \times 25 \times 25$ mm^3 moulds. To avoid the upper layers of the samples rapidly drying out, they were covered with plastic foil. After 24 h, the hardened samples were removed from the mould. The AAM samples were left to cure at room temperature for a minimum of 28 days.

Leaching of uranium and structural elements

To assess the release of the introduced uranium and the structural elements Fe, Al, and Na, a monolithic leaching test based on the standard CEN/TS 15863:2015 [29] was performed, where periodic renewal of the eluate volume is foreseen. The cured AAM samples were measured for dimensions and weight. The samples had two pin-sized

Table 1 Chemical composition of the precursor in wt% measured by XRF, iron oxide and calcium oxide over silica molar ratio, and iron oxide over calcium oxide molar ratio

Fe_xO_y	SiO_2	CaO	Al_2O_3	Other	$(Fe_xO_y + CaO)/SiO_2$	Fe_xO_y/CaO
49.8	34.1	3.4	11.6	1.0	1.56	14.51

Table 2 Time intervals for eluate collection [29]

Step/ fraction	Duration from the start of the test (t_0)
1	6 h ± 15 min
2	1 d ± 45 min
3	2 d and 6 h ± 2 h
4	4 d ± 4 h
5	9 d ± 10 h
6	16 d ± 18 h
7	36 d ± 42 h
8	64 d

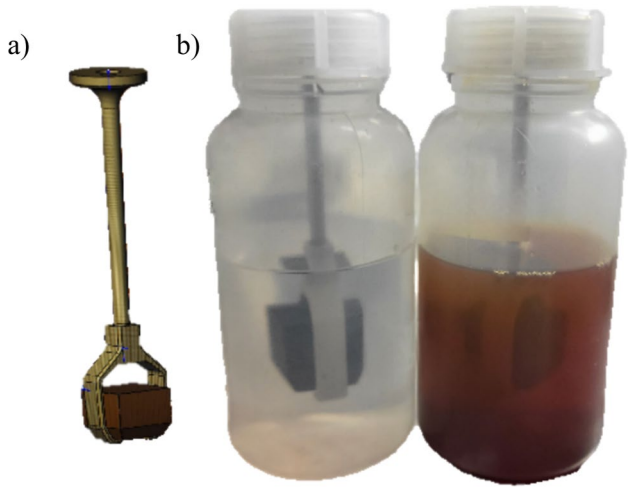

Fig. 2 **a** Sample holder design and **b** experimental leaching setup

contact spots with the sample holder and were fixed in the centre of the leachant volume (250 mL). The material of the bottles was PE, the sample holder was made from PEEK and stainless steel. The containers were tightly closed and were only opened during the collection of eluates at predefined time intervals, which are shown in Table 2. The experimental setup can be seen in Fig. 2.

Two sets of experiments were made, each one in three replicates. In one case the leachant was demineralized water and in the other, the leachant was 0.25 mol L^{-1} nitric acid (HNO_3) with a pH of 0.7 in order to simulate extreme conditions. AAM samples leached in acid are labelled as IPU_NL and the ones leached in water as IPU_WL. In both cases, a blank experiment was performed as well, under the same conditions, excluding the presence of an AAM sample. An eluate of 3 mL was collected, filtered through a 0.45 µm pore-sized syringe filter, and immediately acidified to a concentration of 1 mol L^{-1} HNO_3. The concentration of U, Fe, Al and Na were measured by an inductively coupled plasma mass spectrometry (ICP-MS) instrument (ElementXR, Thermo Fisher Scientific). At each sampling time, the conductivity (Portable Conductivity Meter, METTLER TOLEDO) and pH (MP225 pH Meter, METTLER TOLEDO) of the eluates were measured. The leaching tests were carried out in an under-air glovebox and in laboratory conditions (20 ± 5 °C). Before each leaching test the setup was washed with 0.1 M HNO_3 and then with distilled water.

Fragments of the AAM samples (pristine, leached in water and acid) were collected and crushed in a mortar. Further characterisation was performed at room temperature by powder X-ray diffraction (XRD), Fourier Transform Infrared (FTIR) spectroscopy and Scanning Electron Microscopy (SEM).

XRD analyses were performed on powderised polycrystalline AAM sample material with a Rigaku Miniflex 600 benchtop θ:2θ diffractometer. The system had a 2.0 kW Cu X-ray tube, NaI scintillation counter detector, and graphite monochromator. Instrument control and data processing were performed using a PDXL Comprehensive Analysis Package PC.

FTIR spectroscopy was performed on powderised AAM sample material in attenuated total reflectance mode with an Alpha Platinum Bruker spectrometer equipped with ZnSe crystal. Spectra were obtained in the wavenumber range from 600 to 4000 cm^{-1} with a resolution of 4 cm^{-1}.

Scanning electron microscopy analysis was performed on uncoated fractured surface of the AAM samples using a Thermo Scientific Quattro Scanning Electron Microscope fitted with an Energy-dispersive X-ray spectroscopy (EDS) XFlash 6/30 detector).

Results and discussion

The results of the static leaching tests are analysed to provide a comprehensive understanding of U leaching behaviour from AAM samples. The matrix stability is evaluated under normal and extreme conditions (leached in water and acid, respectively), and the release of U is examined. The structural, chemical, and morphological changes of the AAM samples are investigated before and after the leaching tests with FTIR, XRD, SEM and EDX mapping techniques.

Leaching in water

As seen in Fig. 3 in the first 4 days, the pH rises rapidly while after the 10-day mark and reaches a plateau. In Fig. 4 the release of the structural elements Fe, Na and Al and the contaminant U is shown.

Table 3 shows the total concentration of Fe, Na, Al and U released throughout the leaching test in water in mg L^{-1}

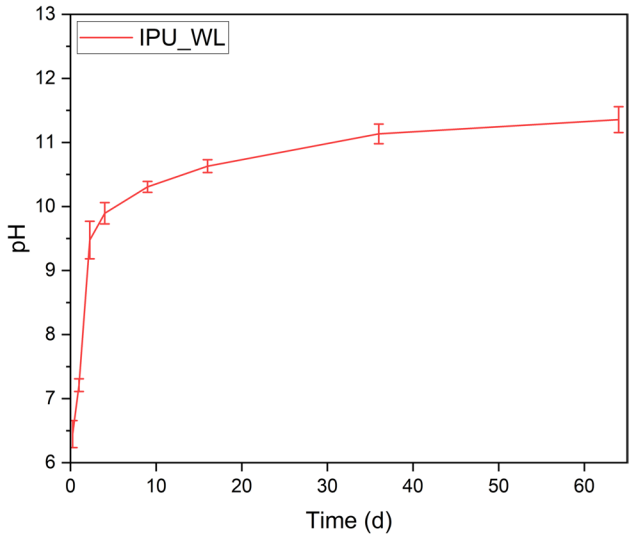

Fig. 3 Evolution of pH during the course of the monolithic static leaching in water experiment

and in mg m^{-2}. The different unit expressions of the results ensure the ability to compare the results to other shapes and sizes of testing portions, the unit mg L^{-1} is only valid for the specimen size and shape tested in this work, while mg m^{-2} can be compared to other testing portions [29]. The leaching of U in the water-leached AAM samples stands at a very low 0.047 mg L^{-1}. The relative uncertainties observed in the results for the water-leached experiment are due to the low concentration levels in these leachates.

Following the CEN/TS 15863 protocol [29] the release mechanism for the elements examined in the experiment was investigated. For Na, diffusion was identified as the main release mechanism, based on the observation that $\sqrt{MSE} < 0.4$, where MSE represents the mean square error of the concentration in eluates 2 to 8. No secondary mechanisms were determined according to the protocol [29]. The release mechanism for Fe, Al and U remain unidentified.

While the speciation of Na remains unaffected by the acidity or alkalinity of solutions, existing as Na^+ in both occasions, Fe, Al and U exist in different forms at different pH levels [30]. The pH of the eluates collected in the leaching of the AAM samples in water ranged between 7–12 (Fig. 3). In alkaline environments, Fe, precipitates as $Fe(OH)_3$, while Al demonstrates amphoteric behaviour, with increasing solubility as $Al(OH)_4^-$ as the pH rises towards alkaline conditions. U shows more complex behaviour. According to the Pourbaix diagram for uranium in non-complexing aqueous media, the main species present in solution would be $UO_2(OH)_3^-$/$UO_2(OH)_4^{2-}$ in the pH range of the

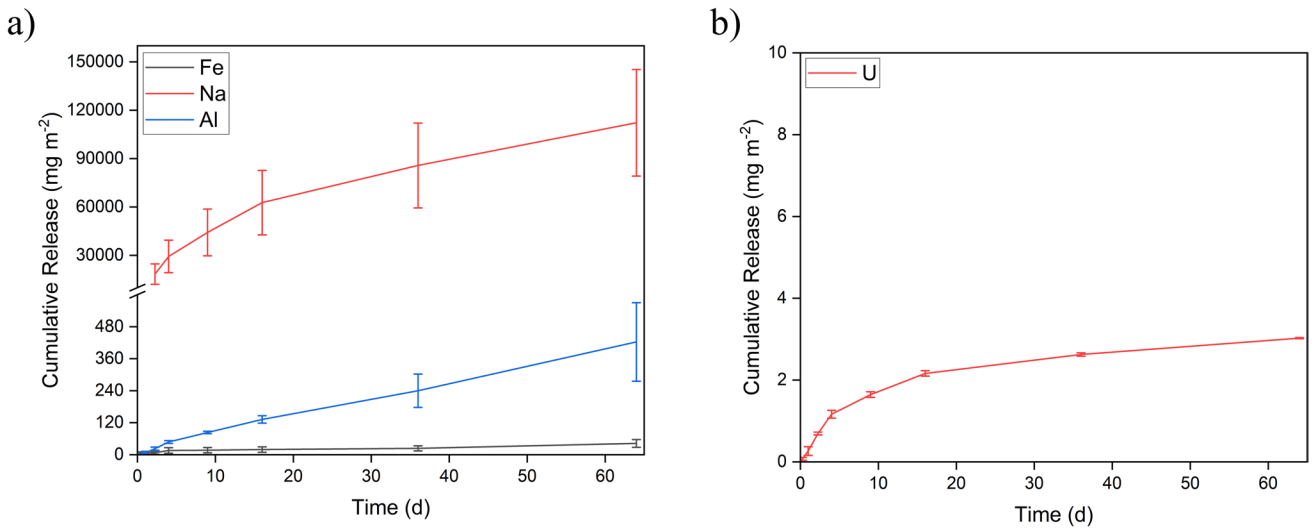

Fig. 4 Cumulative release of **a** structural elements Fe, Na and Al and, **b** contaminant U in the water leaching experiment

Table 3 Cumulative release of Fe, Na, Al and U in sample IPU_WL (leached in water) in mg L^{-1} and in mg m^{-2}. The uncertainties are based on the propagation of the individual analytical results

Concentration units	Fe	Na	Al	U
mg L^{-1}	0.66 ± 0.23	1760 ± 540	6.6 ± 2.2	0.047 ± 0.001
mg m^{-2}	42.50 ± 14.50	(1.10 ± 0.30) × 10^5	(4.20 ± 1.50) × 10^2	3.02 ± 0.01

leaching in water (pH 7–12) [31]. In oxidizing conditions, it forms soluble complexes like $UO_2(CO_3)_3^{4-}$ (uranyl carbonate) or UO_2^{2+} (uranyl ion) [30]. It has been shown that the adsorption of U on AAMs is strongly affected by pH values. When pH increases, more H_3O^+ ions become available from the AAM surface making the sites available to cation exchange with UO_2^{2+} ions [32, 33], which could additionally explain the high retention rate of U in the leaching test performed with water as a leachant.

In order to get more information on the structural changes taking place on the AAM material, FTIR spectra (Fig. 5) were collected before leaching and after leaching. No significant changes were observed between the water-leached and pristine AAM samples. The spectral regions 3735 cm^{-1} (1), 3600–3000 cm^{-1} (2), and 1640 cm^{-1} (3) are known to be related to the O–H stretching bonds and H–O-H bending bonds respectively, both associated with the presence of water in the structures [34]. Bands in the region of 1500 cm^{-1} (4) are associated with the C-O vibrations occurring due to carbonation. These bands are more pronounced in the pristine material that has not been leached, while new bands seem to appear after leaching in the range of 1360 cm^{-1} (5) which are also associated with the C-O vibrations that possibly occur after carbonation [35, 36]. The bands below 1000 cm^{-1} can be attributed to the Si–O vibrations [36, 37]. The spectra remained the same for the area 700 cm^{-1} (9) and corresponds to aluminosilicate phases [38]. Leaching in water had little to no effect on the silicate network.

These results are in line with the XRD analysis which showed that the original AAM sample material is XRD-amorphous with some minor peaks observed that are attributed to aluminium oxides, indicating partial and limited crystallinity. Powder X-ray diffraction measurements of the AAM sample after the leaching experiment demonstrated no changes (results not shown).

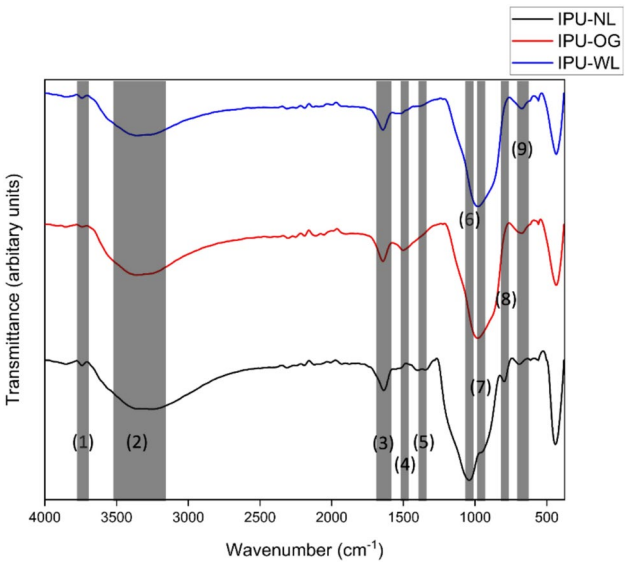

Fig. 5 FTIR spectra of the samples. IPU-OG corresponds to the material that has not been leached while IPU-NL and IPU-WL were leached in acid and water respectively

Figure 6 shows the fracture surface of a non-leached AAM sample, as well as of leached in water AAM sample. Uranium was found as bright aggregates, clearly visible in the images obtained with backscattered electrons (confirmed by EDS), of small particles in the pristine AAM material that was not leached as well as in the AAM sample that were leached in water. EDS analysis did not reveal significant variability in the composition along line scans for the AAM samples that weren't leached and for AAM samples leached in water. The elemental ratio was similar in the bulk of the material and close to the external surface.

Differently from AAM samples not leached, the water-leached AAM samples show extensive matrix cracking (clearly visible in backscattered images). In this case, there are no more obvious differences between bulk and surface layers (the 100 microns mentioned in the not-leached samples). It could mean that the water immersion has enabled a delayed dissolution/gelation/polymerization of the surface.

Figure 7 shows the elemental distribution along a line perpendicular to the external surface of Al, Si and Fe of an AAM sample leached in water; here the proportion of the different elements remains fairly constant in the proximity of the external surface. The profile is also in good agreement with a typical elemental profile of the pristine AAM material before leaching (data not shown). The line scans in Fig. 7 showed no significant variability in terms of material composition along the axis perpendicular to the surface area. The different morphology of the first 100 micron layer could be the result of premature material drying thus preventing a fully developed polymerisation.

Using the ICP-MS measurements, an indicative value of uranium mobilised by water leaching is 0.15%. At this point, we can conclude that the immobilisation efficiency of uranium in such AAMs is 99.85% in normal leaching conditions.

We can tentatively compare these immobilisation yield values with some available in open literature for different waste matrices. Chakrabarty Parta et al. [39] reports cumulative leach fraction of uranium release from rock, uranium tailings, copper kinker ash samples and copper tailings in the range of 0.1–0.4% in distilled water and slightly higher (up to 0.6%) in 0.1N $NaNO_3$ solution. Jian et al. [40] synthesised solidified uranium tailing samples composed from metakaolin and fly ash, and doped with polyvinyl alcohol and basalt fibres. Their material exhibited a 85.25% immobilisation rate of U when leached in distilled water. Despite the experimental conditions being extremely different, we can notice that results usually are in the same order of magnitude.

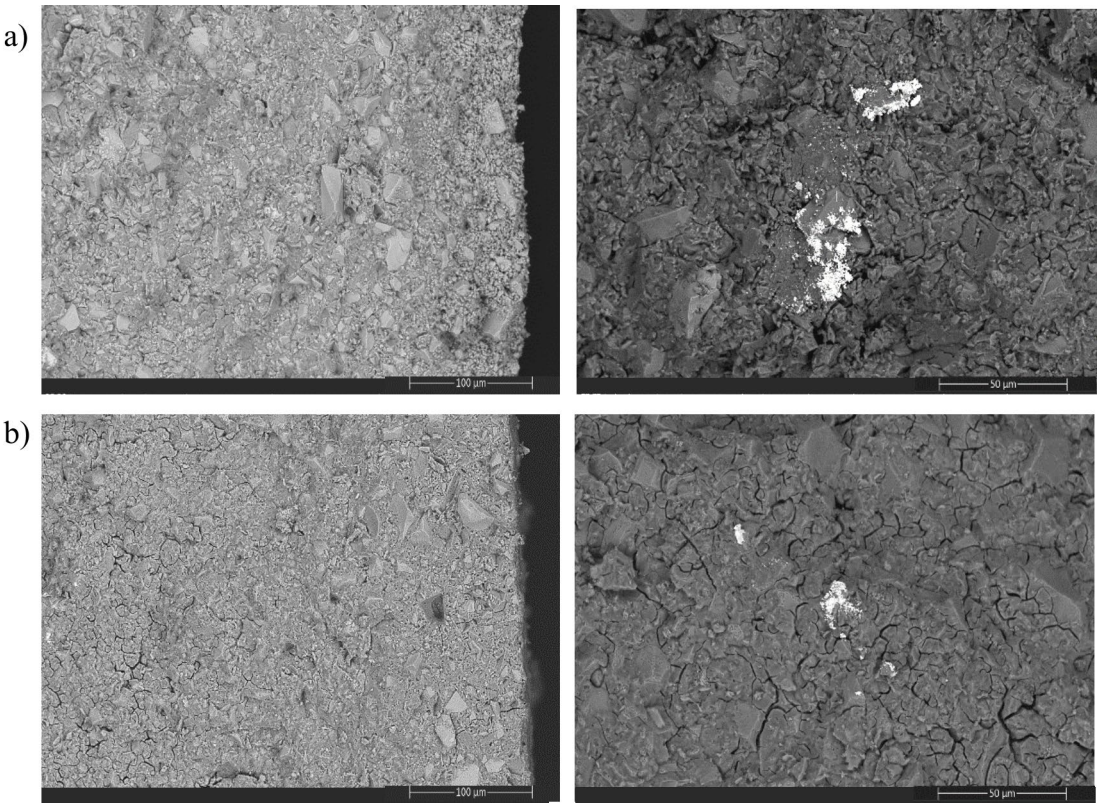

Fig. 6 SEM images of AAM samples **a** that were not leached and AAM samples after being **b** leached in water

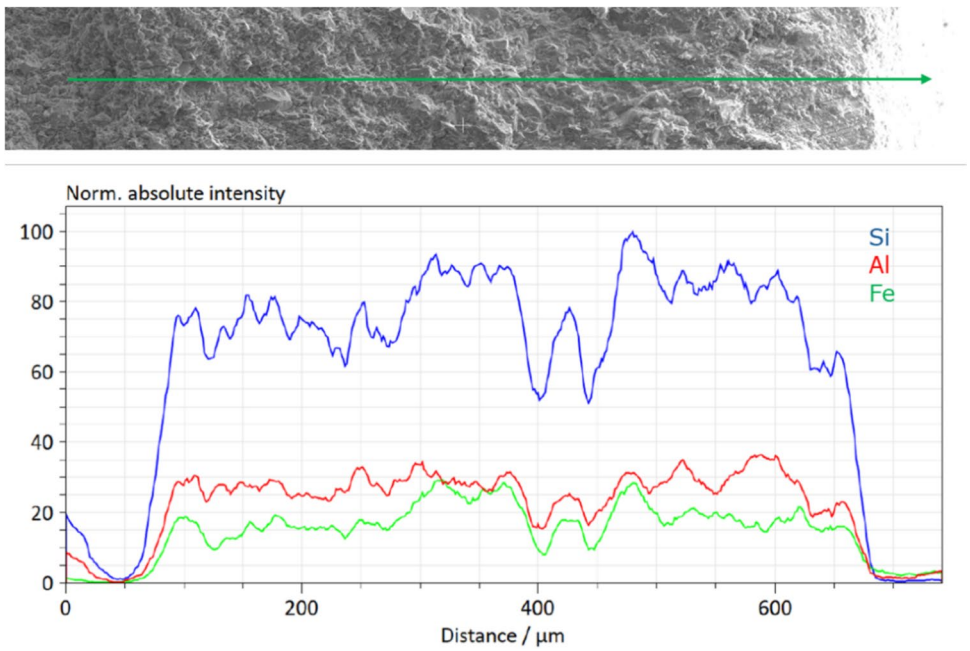

Fig. 7 Line scanning of the peripheral area cross-section of an AAM sample leached in water

Leaching in acid

In order to explore the behaviour of the AAM in extreme conditions and particularly to investigate how well U is bonded in the material, we exposed it to acid in a leaching test. As seen in Fig. 8, much like the samples leached in water, in the first 4 days, the pH rises rapidly until the 10-day mark, after which it plateaus. In Fig. 9 the release of

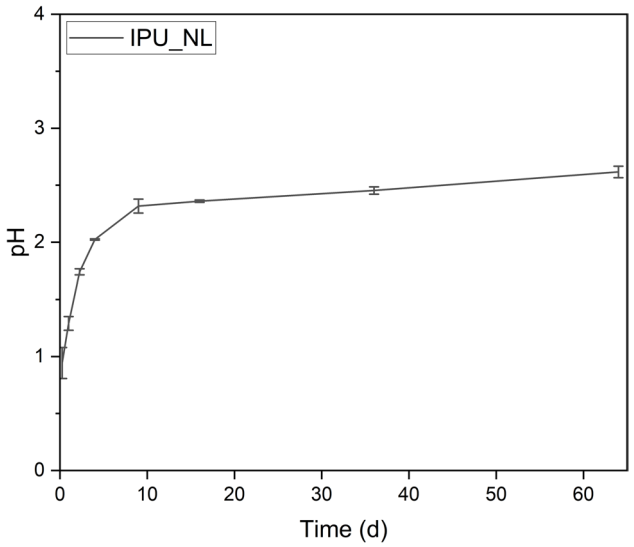

Fig. 8 Evolution of pH during the course of the monolithic static leaching in acid experiment

the structural elements Fe, Na and Al and the contaminant U is shown. As can be observed in Table 4, Fe, Na, Al and U leached respectively 4000, 5, 800 and 30 times more in acid than in water. Similar results were observed regarding the release mechanisms of the examined elements for the leaching experiments performed in nitric acid. For Na, diffusion was confirmed to be the main release mechanism with $\sqrt{MSE} < 0.4$, with no determined secondary mechanisms. The release mechanism for Fe, Al and U remain unidentified also in the leaching tests performed in nitric acid.

An approximate value of uranium mobilized by acid leaching from the cube's volume, as deduced from the ICP-MS measurements, is 5%. However, optical microscopy of the acid leached sample showed the leaching is not homogeneous, as four distinct layers can be seen in Fig. 10, of which the length could be measured. The total depth of penetration of the leaching solution was found to be 0.123 cm. This observation allows us to perform a rough calculation based on the concentrations of uranium in the solid material/leached solution and geometrical considerations. It results in a value of $34 \pm 10\%$ uranium remaining in the penetrated layer leached after two months of leaching in the given experimental conditions. The uncertainty shown here represent an overestimation of combined instrumental and method errors used in this the experiment.

The FTIR spectra of the acid leached material showed changes in the wavelength range of 1360 cm^{-1} (5) (Fig. 5), which, as previously mentioned, is linked to the C-O vibrations that may occur after carbonation due to leaching [35,

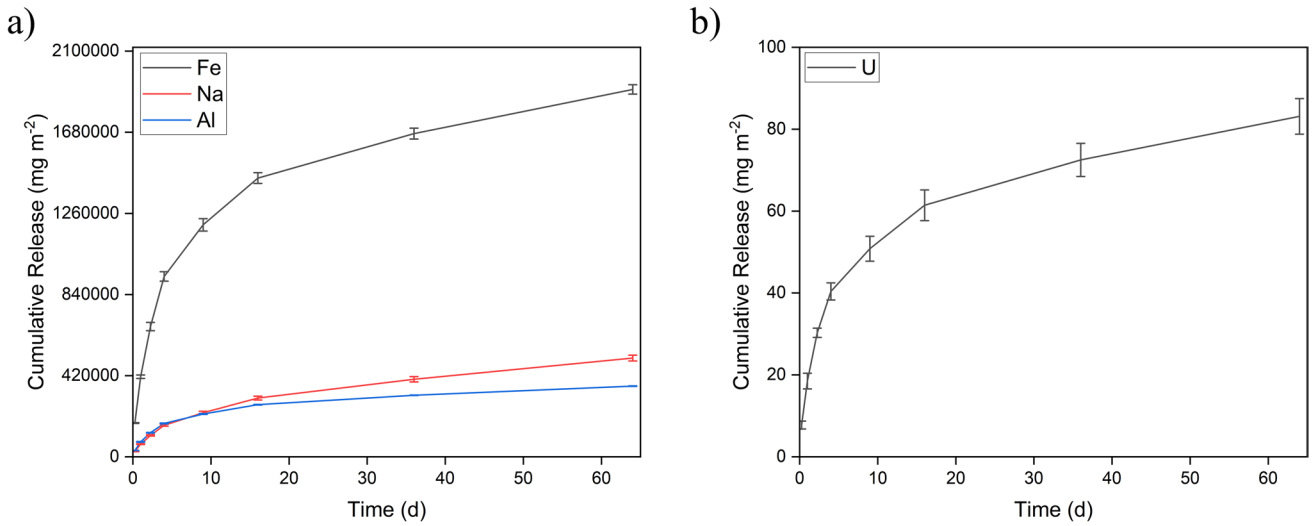

Fig. 9 Cumulative release of **a** structural elements Fe, Na and Al and, **b** contaminant U in the acid leaching experiment

Table 4 Cumulative release of Fe, Na, Al and U in sample IPU_NL (leached in acid) in mg L^{-1} and in mg m^{-2}. The uncertainties are based on the propagation of the individual analytical results

Concentration units	Fe	Na	Al	U
mg L^{-1}	$30{,}050 \pm 390$	8070 ± 240	5780 ± 17	1.310 ± 0.070
mg m^{-2}	$(19.00 \pm 0.25) \times 10^5$	$(5.10 \pm 0.15) \times 10^5$	$(3.70 \pm 0.01) \times 10^5$	83.10 ± 4.30

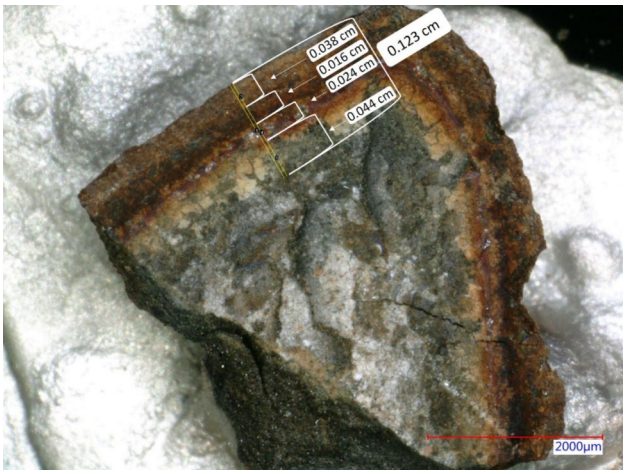

Fig. 10 Image from the inner side of a fragment after the AAM sample was leached in acid

36]. This absorption band also corresponds to the presence of $NaNO_3$ [41] which aligns with its more prominent appearance of it in the AAM sample leached in acid. The leaching in acid seemed to have the biggest impact on the samples´ spectra as a clear shift was observed for the peaks at wavelength 970 cm^{-1} (6) to 1035 cm^{-1} (7) after the experiment. This range is attributed to the Si–O vibrations and the less pronounced peak after leaching in acid indicated degradation of the silicate network. A new peak was noticed at 795 cm^{-1} (8), this region corresponds to iron oxides or the presence of crystalline fayalite [38, 42–44].

Figure 11 depicts a line scan made on the distinct layers seen in Fig. 10 with a direction from the bulk to the external surface of the AAM sample leached in nitric acid solution. From the strong change in the elemental distribution of Al, Fe and Si we conclude that the ferroaluminosilicate network of the AAM sample is influenced, a sign of material degradation.

In the first layer seen in Fig. 12 starting from the surface (50–100 microns), the microstructure seems altered and the glue-like continuous phase is visible everywhere in the bulk is not present and the particles (big and small) seem to be only loosely compacted. This means that the first 100 microns could be more permeable to the water phase. EDS did not show significant signs of uranium uniformly distributed in the AAM material, while it is possibly too low to be detected.

As seen in Fig. 12 U aggregates were no longer observed in the SEM images of the AAM samples leached in acid. This indicates that the U-clusters can be washed out by acid but unlikely by water. This is in good agreement with the solubility of potential uranium compounds, such as UO_{2+x}, U_4O_9 and/or $UO_2(OH)_2{\cdot}H_2O$ [31].

Several studies have also been made testing the immobilisation yield of AAMs in harsh conditions. Zhou et. al [45] investigated the immobilisation yield of U in alkali-activated coal gangue-based geopolymers using acetic acid as a leachate to simulate the leaching process occurring in sanitary landfill environments. They found that the fixation efficiency of U was 77.44%. Li et al. [46] enhanced coal gangue based geopolymers with Nano-hydroxyapatite and tested the materials' ability to retain U using a static and dynamic leaching test and found a 81.73% immobilisation efficiency using acetic acid and deionized water as leachates.

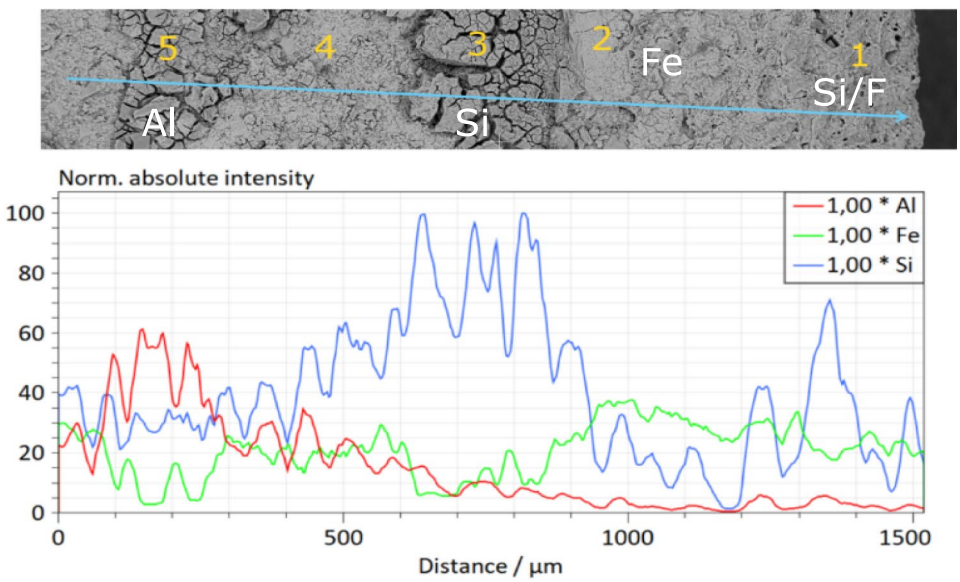

Fig. 11 Line scanning of the peripheral area cross-section of an AAM sample leached in acid

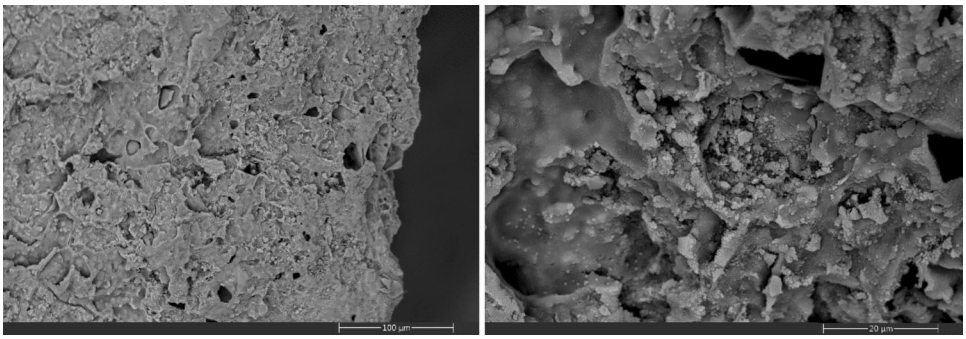

Fig. 12 SEM images of the peripheral region of AAM samples after being leached in acid in different magnifications

Conclusions and outlook

The current study was carried out in order to investigate the feasibility of the use of AAM as a long-term storage solution, namely for the treatment of waste solutions contaminated with uranium. Uranium was found as clusters of uranium in the un-leached AAM samples, and remained there during water-leaching for two months. The fraction of mobilised uranium was extremely low and the uranium levels in the leachates were well under the regulatory limits. The leaching of AAM structural elements was overall at low levels in water, and the structure of the AAM material remained stable, suggesting that AAM immobilisation is a promising alternative to ordinary Portland cement. In case of an extreme environment such as nitric acid solution, uranium was partially leached from the AAM samples in the comparable testing conditions. In this case a barrier was established that slowed down the leaching front into the core of the AAM.

The present results can be extended to the potential qualification of AAMs as matrices for immobilising radioactive and nuclear waste. They can find applications at various stages of the nuclear fuel cycle where treatment aqueous waste liquids would be needed. Further studies on the uranium retention in AAMs would be recommended in order to explore and further validate their potential as nuclear waste immobilisation matrices. Some of the suggested studies would be percolation and pH dependent leaching tests to simulate flowing water scenarios and provide more information on health and environmental risks. Additionally important information could be derived from exposing the AAM samples to irradiation, assessing their durability, morphological changes and leaching levels of the contaminants after irradiation.

Acknowledgements The authors would like to thank Sarah Nourry and Christophe Nourry for their support, Tobias Hertel and Yiannis Pontikes (SREMat) for their help in the production of the slag, Britta Bergfeldt for conducting the XRF measurements in the lab for bulk analysis at the Institute for Technical Chemistry KIT. This work was realised with the collaboration of the European Commission Joint Research Centre under the Collaborative Doctoral Partnership Agreement No 35342.

References

1. United Nations Scientific Committee Committee on the Effects of Atomic Radiation (UNSCEAR), "Sources and effects of ionizing radiation," 1993. [Online]. Available: https://www.unscear.org/unscear/en/publications/1993.html.
2. Manna S, Thakkar UR, Satpati SK, Roy SB, Joshi JB, Chakravartty JK (2016) Study of crystal growth and effect of temperature and mixing on properties of sodium diuranate. Prog Nucl Energy 91:132–139. https://doi.org/10.1016/j.pnucene.2016.03.014
3. Randhawa JS, Robin PK, Meehnian H (2024) A comprehensive review on health and environmental hazards of uranium : analytical techniques, mitigation strategies and its toxicity treatments. J Radioanal Nucl Chem 333(8):3693–3711. https://doi.org/10.1007/s10967-024-09527-1
4. OECD/IAEA, "Environmental Remediation of Uranium Production Facilities," *Nucl. Dev. OECD Publ. Paris*, 2002, https://doi.org/10.1787/9789264194809-en.
5. Kong L, Ruan Y, Zheng Q, Su M, Diao Z, Chen D (2020) Uranium extraction using hydroxyapatite recovered from phosphorus containing wastewater. J Hazard Mater 382:120784. https://doi.org/10.1016/j.jhazmat.2019.120784
6. Ighalo JO et al (2024) Chemosphere a review of remediation technologies for uranium-contaminated water. Chemosphere 352:141322. https://doi.org/10.1016/j.chemosphere.2024.141322
7. J. J. Katz and E. Rabinowitch, 1961 *The Chemistry of Uranium*. Рипол Классик
8. R. Finch and R. Ewing, 1990 "Uraninite alteration in an oxidizing environment and its relevance to the disposal of spent nuclear fuel,"

9. Villagra NR, Milena LJBA, Galán PH (2023) A snapshot review on uranyl secondary phases formation in aqueous systems. MRS Adv 8(6):207–213. https://doi.org/10.1557/s43580-022-00476-z
10. W. E. Falck, *The Long-Term Safety of Uranium Mine and Mill Tailing Legacies in an Enlarged EU*. 2008.
11. Canada Web Standards, "Archived Web Page - Discussion Paper for Public Consultation : DIS-12–02 : Process for Establishing Release Limits and Action Levels at Nuclear Facilities." https://www.cnsc-ccsn.gc.ca/eng/acts-and-regulations/consultation/comment/d-12-02/#P436_44291.
12. Kausar A, Bhatti HN (2013) Adsorptive removal of uranium from wastewater: a review. J. Chem. Soc. Pakistan 35(35):1041–1052
13. IAEA International Atomic Energy Agency, 2004 "Treatment of liquid effluent from uranium mines and mills,".
14. Ferrari CR et al (2017) Effects of the discharge of uranium mining effluents on the water quality of the reservoir : an integrative chemical and ecotoxicological assessment. Sci Rep 7(13919):1–10. https://doi.org/10.1038/s41598-017-14100-w
15. Yokozeki K, Watanabe K, Sakata N, Otsuki N (2003) Prediction of changes in physical properties due to leaching of hydration products from concrete. J Adv Concr Technol 1(2):161–171
16. Sihn Y, Bae S, Lee W (2019) Chemosphere Immobilization of uranium (VI) in a cementitious matrix with nanoscale zerovalent iron (NZVI). Chemosphere 215:626–633. https://doi.org/10.1016/j.chemosphere.2018.10.073
17. Vance ER, Perera DS (2009) Geopolymers for nuclear waste immobilisation. Geopolymers Struct. Process. Prop. Ind. Appl. Elsevier, Amsterdam, pp 401–420. https://doi.org/10.1533/9781845696382.3.401
18. Ojovan MI, Lee WE, Kalmykov SN (2019) Immobilisation of radioactive waste in cement. An Introduction to Nuclear Waste Immobilisation. Elsevier, Amsterdam, pp 271–303
19. Li Q et al (2013) Immobilization of simulated radionuclide 133Cs+ by fly ash-based geopolymer. J Hazard Mater 262:325–331. https://doi.org/10.1016/j.jhazmat.2013.08.049
20. Deja J (2002) Immobilization of Cr6+, Cd2+, Zn2+ and Pb2+ in alkali-activated slag binders. Cem Concr Res 32(12):1971–1979. https://doi.org/10.1016/S0008-8846(02)00904-3
21. Arnout L, Beersaerts G, Liard M, Lootens D, Pontikes Y (2021) Valorising slags from non-ferrous metallurgy into hybrid cementitious binders: mix design and performance. Waste Biomass Valor 12:4679–4694. https://doi.org/10.1007/s12649-020-01322-9
22. Vandevenne N et al (2018) Alkali-activated materials for radionuclide immobilisation and the effect of precursor composition on Cs/Sr retention. J Nucl Mater 510:575–584. https://doi.org/10.1016/j.jnucmat.2018.08.045
23. Vandevenne N et al (2018) Incorporating Cs and Sr into blast furnace slag inorganic polymers and their effect on matrix properties. J Nucl Mater 503:1–12. https://doi.org/10.1016/j.jnucmat.2018.02.023
24. Goo JY, Kim BJ, Kang M, Jeong J, Jo HY, Kwon JS (2021) Leaching behavior of cesium, strontium, cobalt, and europium from immobilized cement matrix. Appl Sci 11(18):8418. https://doi.org/10.3390/app11188418
25. Keulen A, van Zomeren A, Dijkstra JJ (2018) Leaching of monolithic and granular alkali activated slag-fly ash materials, as a function of the mixture design. Waste Manag 78:497–508. https://doi.org/10.1016/j.wasman.2018.06.019
26. Sata V, Sathonsaowaphak A, Chindaprasirt P (2012) Cement & concrete composites resistance of lignite bottom ash geopolymer mortar to sulfate and sulfuric acid attack. Cem Concr Compos 34(5):700–708. https://doi.org/10.1016/j.cemconcomp.2012.01.010
27. Ariffin MAM, Bhutta MAR, Hussin MW, Tahir MM, Aziah N (2013) Sulfuric acid resistance of blended ash geopolymer concrete. Constr Build Mater 43:80–86. https://doi.org/10.1016/j.conbuildmat.2013.01.018
28. Chernorukov NG, Nipruk OV, Kostrova EL (2016) Synthesis and study of sodium uranate Na 2 U 2 O 7 · 6H 2 O and of products of its dehydration and thermal decomposition. Radiochemistry 58(2):124–127. https://doi.org/10.1134/S106636221602003X
29. European Committee for Standardization, "CEN/TS 15863:2015, Characterization of waste - Leaching behaviour test for basic characterization - Dynamic monolithic leaching test with periodic leachant renewal, under fixed conditions," 2015.
30. A. I. Science, "Atlas of Eh-pH diagrams Intercomparison of thermodynamic databases," no. 419, 2005.
31. K. M. Krupka and R. J. Serne, 2002 "Geochemical Factors Affecting the Behavior of Antimony , Cobalt , Europium , Technetium , and Uranium in Vadose Sediments,"
32. Wang G, Wang X, Chai X, Liu J, Deng N (2010) Applied clay science adsorption of uranium (VI) from aqueous solution on calcined and acid-activated kaolin. Appl Clay Sci 47(3–4):448–451. https://doi.org/10.1016/j.clay.2009.11.003
33. Parab H, Joshi S, Shenoy N, Verma R (2005) Uranium removal from aqueous solution by coir pith : equilibrium and kinetic studies. Bioresour Technol 96:1241–1248. https://doi.org/10.1016/j.biortech.2004.10.016
34. A. Peys, L. Arnout, H. Tobias, and I. Remus Ion, 2017 "The use of ATR-FTIR spectroscopy in the analysis of iron-silicate inorganic polymers," *5th Int. Slag Valoris. Symp.*, no. April,.
35. Bernal SA, Provis JL, Brice DG, Kilcullen A, Duxson P, Van Deventer JSJ (2012) Accelerated carbonation testing of alkali-activated binders signi fi cantly underestimates service life : the role of pore solution chemistry. Cem Concr Res 42(10):1317–1326. https://doi.org/10.1016/j.cemconres.2012.07.002
36. Onisei S, Douvalis AP, Malfliet A, Peys A, Pontikes Y (2018) Inorganic polymers made of fayalite slag: on the microstructure and behavior of Fe. J Am Ceram Soc 101(6):2245–2257. https://doi.org/10.1111/jace.15420
37. Mysen BO, Virgo D, Neumann ER, Seifert FA (1985) Redox equilibria and the structural states of ferric and ferrous iron in melts in the system CaO-MgO-Al2O3-SiO2- Fe- O: relationships between redox equilibria, melt structure and liquidus phase equilibria. Am Mineral 70(3–4):317–331
38. Hertel T, Blanpain B, Pontikes Y (2016) A proposal for a 100 % use of bauxite residue towards inorganic polymer mortar. J Sustain Metall 2(4):394–404. https://doi.org/10.1007/s40831-016-0080-6
39. Chakrabarty Patra A, Sumesh CG, Mohapatra S, Sahoo SK, Tripathi RM, Puranik VD (2011) Long-term leaching of uranium from different waste matrices. J Environ Manage 92(3):919–925. https://doi.org/10.1016/j.jenvman.2010.10.046
40. Jiang F et al (2022) Preparation and related properties of geopolymer solidified uranium tailings bodies with various fibers and fiber content. Environ Sci Pollut Res 29:20603–20616. https://doi.org/10.1007/s11356-021-17176-0
41. M. Camaiti, M. Bacci, and M. Picollo, "15 . The identification of nitrates on carbonate substrates using diffuse reflectance infrared Fourier Transform DRIFTs in CaF 2 Matrix," *POSTPRINTS,* pp. 127–134, 1998.
42. Hofmeister AM (1997) Infrared reflectance spectra of fayalite, and absorption data from assorted olivines, including pressure and isotope effects. Phys Chem Miner 24(7):535–546. https://doi.org/10.1007/s002690050069

43. Hofmeister AM (1987) Single-crystal absorption and reflection infrared spectroscopy of forsterite and fayalite. Phys Chem Miner 14(6):499–513. https://doi.org/10.1007/BF00308285
44. Lafuente B, Downs RT, Yang H, Stone N (2016) The power of databases The RRUFF project. In: Armbruster T, Danisi RM (eds) Highlights Mineral Crystallogr. De Gruyter, Berlin, pp 1–29. https://doi.org/10.1515/9783110417104-003
45. Zhou S et al (2021) Immobilization of uranium soils with alkali - activated coal gangue – based geopolymer. J Radioanal Nucl Chem 329:1155–1166. https://doi.org/10.1007/s10967-021-07812-x
46. Li J et al (2021) Immobilization of uranium soil by geopolymer coupled with nHAP. Ceram Int 47:30815–30825. https://doi.org/10.1016/j.ceramint.2021.07.262